Mon. Not. R. Astron. Soc. **000**, 1–13 (2013) Printed 22 January 2014 (MN LATEX style file v2.2)

Establishing an analogue population for the most distant galaxies

Elizabeth R. Stanway[1⋆] and Luke J. M. Davies[2,3]
[1] *Department of Physics, University of Warwick, Gibbet Hill Road, Coventry, CV4 7AL, UK*
[2] *H. H. Wills Physics Laboratory, University of Bristol, Tyndall Avenue, Bristol, BS8 1TL, UK*
[3] *ICRAR, The University of Western Australia, 35 Stirling Highway, Crawley, WA 6009, Australia*

arXiv:1401.5059v1 [astro-ph.GA] 20 Jan 2014

ABSTRACT
Lyman break analogues (LBAs) are local galaxies selected to match a more distant (usually $z \sim 3$) galaxy population in luminosity, UV-spectral slope and physical characteristics, and so provide an accessible laboratory for exploring their properties. However, as the Lyman break technique is extended to higher redshifts, it has become clear that the Lyman break galaxies (LBGs) at $z \sim 3$ are more massive, luminous, redder, more extended and at higher metallicities than their $z \sim 5$ counterparts. Thus extrapolations from the existing LBA samples (which match $z = 3$ properties) have limited value for characterising $z > 5$ galaxies, or inferring properties unobservable at high redshift. We present a new pilot sample of twenty-one compact star forming galaxies in the local ($0.05 < z < 0.25$) Universe, which are tuned to match the luminosities and star formation volume densities observed in $z \gtrsim 5$ LBGs. Analysis of optical emission line indices suggests that these sources have typical metallicities of a few tenths Solar (again, consistent with the distant population). We also present radio continuum observations of a subset of this sample (13 sources) and determine that their radio fluxes are consistent with those inferred from the ultraviolet, precluding the presence of a heavily obscured AGN or significant dusty star formation.

Key words: galaxies: evolution – galaxies: high redshift – galaxies: star formation - radio continuum: galaxies – ultraviolet: galaxies

1 INTRODUCTION

Lyman break analogues (LBAs) are a class of compact, UV-luminous galaxies in the local universe that are selected to match the more distant Lyman break galaxy (LBG) population in luminosity, UV-spectral slope and physical characteristics. Lyman break galaxies are named for their dominant spectral feature - a strong rest-frame ultraviolet continuum, which demonstrates a significant flux decrement at the wavelengths corresponding to 912Å and 1216Å in the galaxy rest-frame. Below 912Å photons are sufficiently energetic to ionise neutral Hydrogen in the intergalactic medium and so are efficiently scattered from the line of sight before reaching the observer. Between 912Å and 1216Å the same intergalactic medium can also scatter light in narrow absorption lines representing electron transitions in the Lyman series of Hydrogen (particularly Lyman-α). Given that the density of gas clouds in the intergalactic medium rises sharply with increasing redshift, and each cloud absorbs at wavelengths corresponding to its own redshift, the resulting 'forest' of redshifted lines can lead to a significant amount of flux lost from the line of sight.

At $z \sim 3$, the cumulative effect of scattering in Lyman-α forest leads to a sharp break in the spectrum, such that about half the flux shortwards of 1216Å is lost and below the second break at 912Å reduces to negligible levels. Thus a source will appear absent in a photometric image taken in a filter lying below this wavelength and is said to have "dropped-out". Therefore $z \sim 3$ Lyman break galaxies, identified by their broadband imaging, are termed "U-dropouts" or sometimes "U-drops". At higher redshifts still, the Lyman-α forest is denser, with the decrement across 1216Å in the rest frame exceeding 90%, and the break has moved to higher observed wavelengths. Thus $R-$drops can be selected at $z \sim 5$, $I-$drops at $z \sim 6$ and so on.

While rest-frame ultraviolet-selected LBGs are our primary source for understanding galaxy formation and the 'normal' galaxy population in the distant Universe, our knowledge of them is necessarily limited by their faint apparent magnitudes, small projected sizes, and extreme redshifts. The interpretation of these galaxies can be greatly enhanced by the consideration of local analogues for which more extensive and more detailed data can be obtained.

⋆ E-mail: e.r.stanway@warwick.ac.uk

© 2013 RAS

The study of local galaxies as potential LBAs has developed rapidly over recent years. Heckman and collaborators have built on their early work (Heckman et al. 2005; Hoopes et al. 2007), identifying a sample of ultra-compact, ultraviolet-luminous galaxies that are a close mirror to $z \sim 3$ LBGs. Such sources are selected in data from the Galaxy Evolution Explorer (GALEX) survey and subsequent studies have explored their properties in infrared photometry (e.g. Izotov et al. 2011), X-rays (Jia et al. 2011), ultraviolet spectroscopy (Heckman et al. 2011) and morphology (e.g. Overzier et al. 2011).

However, work by Haberzettl et al. (2012) and others has shown the importance of consistency in selection techniques across redshift. Recent colour selected samples of $z \sim 2$ candidates such as the BX/BM samples have been described as 'Lyman break galaxies' but are in fact selected based on rest-frame optical, rather than ultraviolet colours (Steidel et al. 2004). As Haberzettl et al. (2012) found, this difference in selection technique, while identifying galaxies at the predicted redshift, biases galaxy samples towards a quantitatively different population. Similarly $z = 0.2$ 'Green Peas' (star forming galaxies selected for their strong rest-frame optical emission lines and compact morphology, Cardamone et al. 2009) are distinct from analogues selected from rest-UV photometry at the same redshift (e.g. Heckman et al. 2011). While all the galaxies identified by these techniques are actively star-forming, their derived properties such as star formation rate, dust extinction, stellar population age, physical size and hence physical conditions can be very different. Given that each of these populations is deemed, in certain ways, characteristic of its redshift, it becomes increasingly difficult to interpret comparisons between these discrepant populations as indicative of evolution either in the building blocks of today's massive galaxies or of wider volume-averaged cosmological properties. It is vital that the criteria used to identify galaxy populations to be compared at different redshifts are as close as possible to being identical.

As the Lyman break technique is extended to ever higher redshifts (e.g. Douglas et al. 2010, 2009; Bouwens et al. 2012, 2007), it has become increasingly clear that the LBA population identified by Heckman and coworkers, and the 'Green Pea' selection of Cardamone et al, provides a poor match for the properties of high redshift ($z > 5$) UV-selected galaxies. Selected to match the typical properties of $z \sim 3$ LBGs, they are too massive and often too red to provide a good comparison to existing $5 < z < 8$ samples, which are less luminous ($L*_{z=6} \sim 0.3L*_{z=3}$, e.g. Bouwens et al. 2007), younger and less massive ($\sim 30\,\mathrm{Myr}$, $M_{\mathrm{stellar}} \sim \mathrm{few} \times 10^9\,M_\odot$, e.g. Verma et al. 2007, although c.f. Oesch et al 2013) and at lower metallicities ($Z \sim 0.2 - 0.5 Z_\odot$, e.g. Douglas et al. 2010) than their $z \sim 3$ counterparts. Curiously, galaxies that may act as plausible analogues for exceptionally low-metallicity star-forming galaxies (touted as being appropriate for the very earliest galaxies at $z > 9$, but yet to be observationally confirmed) have received more attention (e.g. Izotov et al. 2011) than those at a few tenths of solar, as appropriate to $z \sim 5 - 7$. LBGs at $z > 5$ are also significantly more compact than their lower redshift counterparts (Oesch et al. 2010), driving the star formation density (both in terms of volume and per unit stellar mass) to levels not seen in the equivalent $z = 3$ population. This higher star formation density is a key observational driver for searching for better analogues. Higher UV-photon density changes the physical conditions within the galaxies. Dust temperatures are likely to be higher, the intergalactic medium warmer, and hence the collapse of molecular clouds into stars, the ionization of the intergalactic medium and potentially the mode of star formation itself rather different. Thus analogues with lower star formation rate density (as typical for the $z = 3$ population) simply *cannot* provide good physical models with which to understand galaxies in the very distant universe. If LBAs are to inform our understanding at $z \geqslant 5$, or extrapolate from the UV-luminous component, then a specialized $z \sim 5$-equivalent LBA population must be established.

Through a combination of archival work and proprietary observations, we have developed a sample of spectroscopically-confirmed, star-forming, $z = 0.05 - 0.20$ galaxies identified in the UV and optical (using GALEX DR6 and the SDSS DR7), that we are exploring in detail as analogues for the $z > 5$ population. In this paper we discuss the properties of a plausible candidate Lyman Break analogue galaxy sample, tuned to match the physical properties of the observed $z \geqslant 5$ galaxy population. In section 2 we identify the sample under discussion, exploring their properties in the SDSS optical survey in section 3. In section 4 we present new radio imaging of a subsample of objects and discuss the results, before extending the discussion to the implications of the sample more generally in section 5.

Throughout, optical magnitudes are presented in the AB system. Where necessary, we use a standard ΛCDM cosmology with $H_0 = 70\,\mathrm{km\,s^{-1}\,Mpc^{-1}}$, $\Omega_M = 0.3$ and $\Omega_\Lambda = 0.7$.

2 CANDIDATE SELECTION

2.1 Motivation

While it has become clear that the intrinsic properties of the Lyman break galaxy population evolves with redshift, it has not been clear whether the Lyman break analogue candidate samples already suggested or investigated is sufficiently broad to encompass a subset of good $z > 5$ analogue systems.

We explored this question using the largest, best developed LBA sample: that identified by Heckman et al. (2005) and expanded in Hoopes et al. (2007)[1] and related work. These sources were selected based on a combination of UV luminosity and UV-optical colour to mirror the properties of the $z = 3$ Lyman break galaxy population, with the primary selection based on UV flux (and hence inferred star formation rate) exceeding $\sim 0.3\,L_\odot$ for $z = 3$ LBGs (Hoopes et al. 2007). The galaxies occupy a redshift range of $0.08 < z < 0.30$, with a mean of $z = 0.20$. No constraint was placed on the angular size of the systems. However, projected size (after deconvolution with the seeing) was available from SDSS data.

One of the primary drivers for identifying analogues to

[1] While the Hoopes et al targets were primarily identified as ultraviolet-luminous galaxies (UVLGs), they were nonetheless motivated as an LBA sample.

distant sources is to explore the effects of very high volume-averaged star formation densities, as discussed above. In figure 1, we calculate the inferred star formation density (assuming that the observed star formation is concentrated within the observed half-light radius of the galaxy) for the catalogue of Hoopes et al. (2007) and compare it to the derived typical values for Lyman break galaxy samples at high redshift, using the Schecter parameter M* (from Bouwens et al. 2007) as a typical luminosity and the mean physical half light radius at each redshift from Oesch et al. (2010). Star formation rates are calculated from the rest-frame ultraviolet flux density, using the conversion factor of Madau, Pozzetti, & Dickinson (1998), $L_{UV} = 8.0 \times 10^{27}\,(\mathrm{SFR}\,/\,\mathrm{M}_{\odot}/\mathrm{yr})\,\mathrm{ergs\,s^{-1}\,Hz^{-1}}$, assuming a Salpeter IMF. As is often the case for work on Lyman break galaxies at $z \gtrsim 5$, no correction is made for dust extinction of the ultraviolet flux (which is essentially unknown at $z > 5$) or any change in the IMF with redshift. Given that dust extinction at $z \sim 3$ can be as much as factor of a few, the inferred star formation rates are considered to be lower limits, and the star formation densities may be still higher than shown - however observations in the thermal far-infared and submillimeter would be required to reliably determine a total star formation rate - challenging even for ALMA at $z \sim 5$. The rationale here is to compare like for like - observed ultraviolet luminosity for observed ultraviolet luminosity - and investigate dust properties when a sample for investigation has been defined. As the figure clearly demonstrates, very few of the Hoopes et al analogue sample (∼3%) have a star formation density comparable to that observed in distant Lyman break galaxies - a discrepancy that only becomes exacerbated as the Lyman break samples are pushed to ever higher redshifts.

Figure 1 also illustrates a second concern with the use of previously identified local, luminous starbursts as Lyman break analogues: the increasingly low luminosities being probed by deep and distant surveys. The typical luminosity of Lyman break galaxies is firmly established to evolve with increasing redshift, being some 1.5 magnitudes fainter at $z \sim 7$ than at $z \sim 3$ (e.g. Wilkins et al. 2011). Even setting aside evolution in the physical size distribution of these sources, it is clear that finding analogues for $z \geqslant 5$ galaxies identified in surveys such as CANDELS (Grogin et al. 2011, which is probing 120 arcmin^2 to a uniform depth of ∼27.5 in ten broad wavebands) will require the study of less luminous and more compact galaxies than previously considered.

2.2 Selection criteria

We have explored the public data releases from the Sloan Digital Sky Survey (DR7, Abazajian et al. 2009) in the optical (*ugriz* bands), and GALEX (GR6[2]) in its two ultraviolet bands (FUV and NUV, centred at 1538Å and 2315Å respectively) for systems that might satisfy this requirement. In order to tune our sample to better match the high redshift population, we apply several selection criteria:

Colour: Where Heckman et al. (2005) use the fairly liberal UV-to-optical criterion of $FUV - r < 2$, suitable for identifying continuous star formation over timescales of several hundred years, we do not rely on optical colours but rather apply a tight constraint in the UV - analogous to a high redshift LBG selection. Beyond $z = 5$, the rest-frame optical is shifted well into the infrared and difficult to observe. Hence candidate selection is performed through a combination of a strong spectral break at 1216Å (due to absorption in the intervening intergalactic medium, e.g. Bouwens et al. 2007; Bremer et al. 2004; Stanway, Bunker, & McMahon 2003) and a flat or relatively blue spectral slope observed as a small photometric colour between bands in the rest-frame ultraviolet (Wilkins et al. 2013; Stanway, McMahon, & Bunker 2005).

To mirror this, we require that the rest-UV slope is very close to flat (i.e. $FUV - NUV < 0.5$), targeting galaxies with young starbursts of <200 Myr (see figure 2). We must, of course, allow for some range of dust extinction in the population. Verma et al. (2007) found that the spectral energy distribution of $z \sim 5$ galaxies are best fit with $A_V \sim 0.3$ mag, a little lower than that measured at $z \sim 3$ ($A_V \sim 0.5$ mag, Shapley et al, 2003). Evidence from the rest-frame ultraviolet slopes of candidate samples suggest Lyman break galaxies at higher redshift may have still lower extinctions, but with considerable uncertainties (see Wilkins et al. 2013, for a detailed discussion). To accommodate this variation, we do not explicitly constrain the $NUV - r$ band colour, allow-

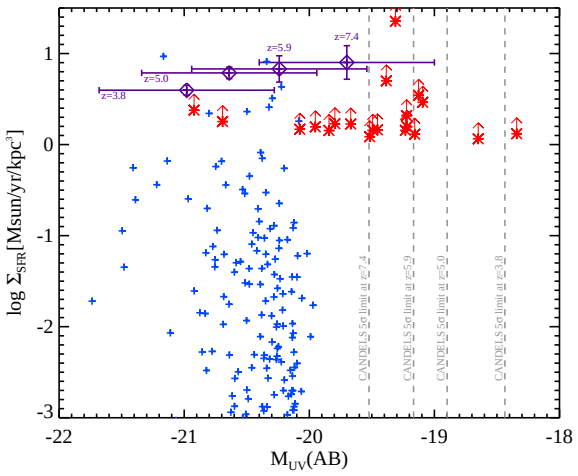

Figure 1. The star formation density as function of luminosity for LBG samples at high redshift (diamonds), the LBA sample of Hoopes et al (2007, crosses) and the sample discussed in this work (asterisks). The current sample are shown as lower limits since all are essentially unresolved in SDSS data. We calculate the inferred star formation density from the observed 1500Å flux and SDSS morphology, assuming for simplicity that the observed star formation is concentrated within a cube with a scale length given by the observed half-light radius of the galaxy (note that a spherical assumption would change each value by a factor of 4π). For LBG samples, we use the typical absolute magnitudes determined by Bouwens et al (2007), and typical sizes from Oesch et al (2010) from deep, space-based dropout samples. The horizontal ranges on these points indicate a factor of 2 in luminosity, either side of the typical luminosity M*. We also show the limits in absolute magnitude corresponding to the 'Deep' CANDELS survey target depths of 27.5 AB. The standard conversion factor of Madau et al 1998 ($L_{UV} = 8.0 \times 10^{27}\,(\mathrm{SFR}\,/\,\mathrm{M}_{\odot}/\mathrm{yr})\,\mathrm{ergs\,s^{-1}\,Hz^{-1}}$, using a Salpeter IMF) is assumed.

[2] Available at http://galex.stsci.edu/GR6/

ing for variations in stellar population age within the sample, and moderate dust extinction. However we note that no plausible candidates had colours redder than $NUV-r = 2.2$.

Luminosity: We tune our selection window to FUV absolute magnitudes which are equivalent to those in existing $z > 5$ LBG samples. This requires that we probe galaxies with L_{UV}=0.1 − 5 $L*_{z=6}$, where M^*_{UV}=-20.24 at $z = 6$ (Bouwens et al. 2007).

Size: We also require that this star formation occurs in a compact region (distant galaxies have a projected half-light radius < 2 kpc, Oesch et al. 2010), so as to ensure a similar star formation volume density in the local analogue systems to that observed in the high redshift sources. Given the typical seeing of SDSS images, deconvolution of very compact sources to determine their physical size is problematic. At $z > 0.2$, a physical size of 2 kpc is identified as only a small perturbation on the light profile due to average seeing. Thus the requirement that the SDSS pipeline is able to constrain the size effectively provides an upper limit on our redshift distribution. Given the uncertainties on deconvolution of these objects, we apply the reasonably liberal criteria that the best fit deconvolution corresponds to a physical scale $r < 3.5$ kpc, and that the SDSS g-band petrosian radius is $< 1.2''$. While this may admit a fraction of sources more extended than those at high redshift, as figure 1 shows these lower limits select a population with star formation densities comparable to those observed in the distant Universe. Note that we must constrain the physical size in the optical, since GALEX does not have sufficient resolution in the UV.

Additional Constraints: In order to identify a useful pilot sample for further study we require that our candidates have SDSS spectroscopy, and that this spectroscopy identifies their UV luminosity as arising from star formation rather than AGN (the AGN fraction in distant galaxy samples is known to be very small, Douglas et al. 2007; Nandra, Laird, & Steidel 2005). In the interests of further, ground-based follow-up, we also place a declination constraint (dec < −8.5 deg) to optimize availability to southern telescopes (e.g. ATCA, VLT, ALMA etc.). We eliminate catalogue sources with obvious problems with their photometry (e.g. small clumps which form part of a much larger, more extended system, or objects whose photometry is affected by near neighbours - a particular problem for these faint targets in the GALEX data).

These criteria identify a sample of just 21 sources to investigate in detail, as a subset of the larger, unrestricted declination, population. As figure 1 (and also section 3) demonstrates, these occupy a region of parameter space distinct from that considered by previous studies - both in luminosity and in star formation density. Unsurprisingly these are both fainter in apparent magnitude, and at a slightly lower typical redshift than those of the Hoopes et al. (2007) sample (see figure 3).

3 PROPERTIES IN THE GALEX/SDSS DATA

3.1 UV slope and optical morphology

The selection criteria discussed in section 2 essentially select sources which are unresolved in the optical, as figure 4 shows.

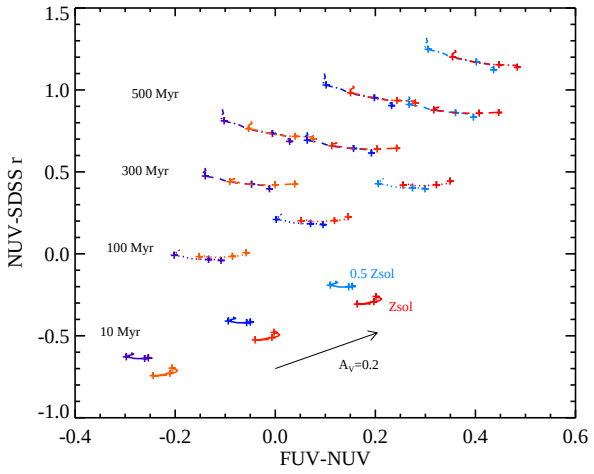

Figure 2. Ultraviolet-optical colours expected of young starburst stellar populations at $0 < z < 0.3$ (increments of $\Delta z = 0.1$ are marked with crosses on each evolutionary track). We use Maraston (2005) stellar population synthesis models for a declining initial starburst to determine the expected colour at four ages, and two metallicities and also show the effects of dust reddening with an A_V=0.2, 0.4, assuming a Calzetti et al. (2000) extinction law. Increasing stellar population age primarily effects the UV-optical colour, while the effects of dust are larger in the ultraviolet. A selection criterion of $FUV - NUV < 0.5$ encompasses the bulk of young stellar populations and reasonable dust extinctions in the local Universe.

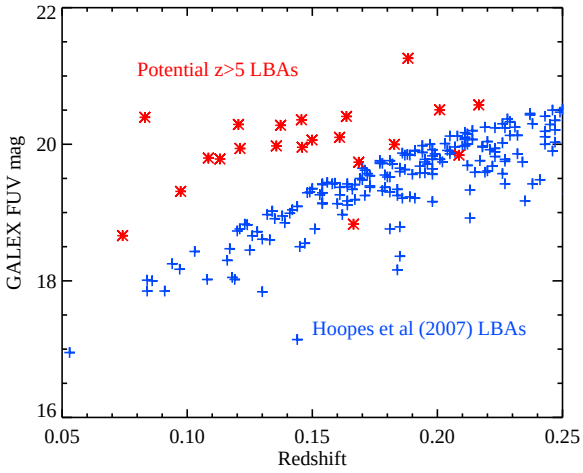

Figure 3. The redshift-apparent magnitude distribution of our targets, compared to the ultraviolet-luminous galaxy sample of Hoopes et al (2007). While there is some overlap, our targets are typically fainter, and at a slightly lower mean redshift.

However a few objects are selected for which the properties of a dominant central core satisfy our selection criteria, but which consist of multiple compact components or possess a slightly more extended, low surface brightness tail. Given that multiple components are often seen in $z \sim 5$ samples (e.g. Douglas et al. 2009), and that low surface brightness emission may well be undetectable at high redshifts, we retain these sources in our sample, in order to explore the full

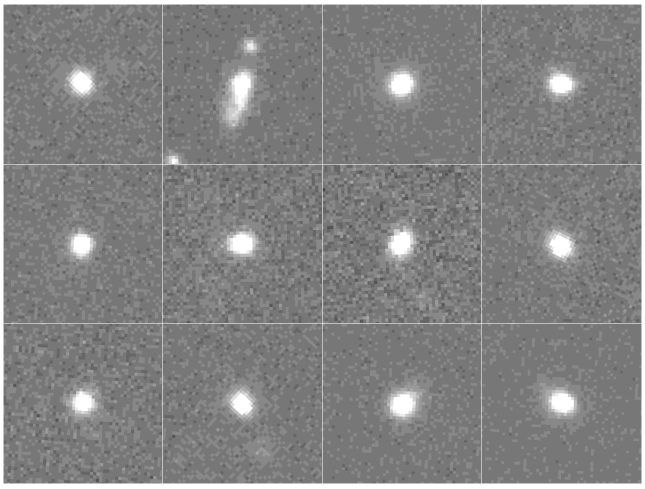

Figure 4. Examples of the essentially unresolved optical morphology (SDSS g band) of these candidates. Boxes are $10''$ on a side. A few objects (for example, the second here) show more extended structure around a central core, and these may prove not to be ideal high redshift analogues, but they are included in the sample so as to explore the range of galaxies identified in catalogue data. Deconvolution suggests a typical half-light radius of <0.5 arcsec.

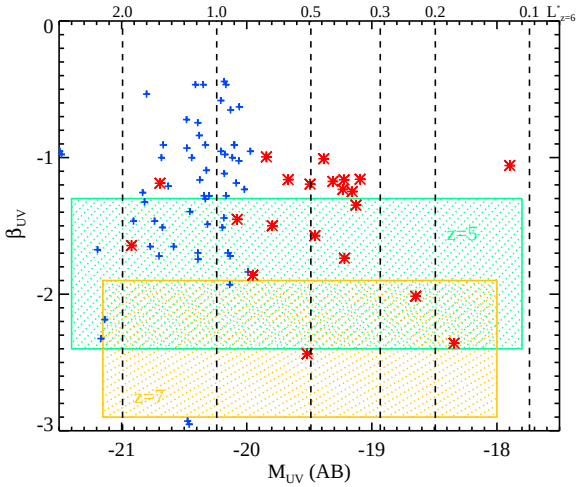

Figure 5. A comparison of the $z \sim 3$ LBA population (crosses), with the sample discussed here (shown as asterisks). The sample presented here forms a distinct and separate galaxy population, probing the lower luminosities, higher star formation densities and sometimes bluer rest-UV colours typical of the high-z population. Shaded regions indicate the range of parameter space that has been estimated by varied authors for LBG samples at $z = 5$ and $z = 7$ (see Wilkins et al. 2013).

properties of this colour-selected population. Further observations (using either adaptive optics or space-based data) will be required to fully constrain the morphology of these sources.

Each source in our sample has a full suite of UV-optical photometry. We use GALEX photometry (at 1300 and 2400Å) and redshift information from SDSS spectroscopy, to explore the observed rest-frame ultraviolet spectral slope of our sample. The observed spectral slope is primarily dependent on a combination of stellar population age and dust extinction, with the bluest colours ($f_\lambda \propto \lambda^\beta$, $\beta < -2$) only possible with zero dust and very low metallicities (see figure 2, and also Wilkins et al 2013 for a fuller discussion). In common with the high redshift samples with which we ultimately wish to compare, we are unable to straightforwardly disentangle the effects of dust and stellar population from a single colour, but instead consider the observed range of values, with a full analysis of dust deferred until more data is available (see discussion later). Even without separating dust and stellar population age, their combined effect is an important indicator of the properties of a galaxy, and has drawn recent attention.

Some authors (e.g. Bouwens et al. 2013, 2012; Ono et al. 2010) have suggested that galaxies at the highest redshifts ($z > 7$) are systematically bluer than those observed at later times and can have extreme spectral slopes, with $\beta < -3$. Such a blue slope is difficult to produce using normal stellar population models and may imply the presence of very low metallicity or Population III stars. However this observation is subject to significant uncertainties and the colours are likely less extreme than originally suggested (see Wilkins et al. 2013, for detailed discussion). Finkelstein et al. (2012), considering the same data as Bouwens et al. (2012), suggested that the spectral slope, while evolving to bluer colours between $z \sim 4$ and $z \sim 7$, does not require such exotic stellar populations. By contrast, Dunlop et al. (2013) have suggested that there's no strong evolution in the slope beyond $z \sim 4$ and that while the colours are typically blue ($\beta \sim -2$), they can be straightforwardly explained with low dust, or slightly sub-solar metallicity, populations. Interestingly, some studies at intermediate redshift ($z < 4$) have found relatively little evidence for a systematic and linear colour evolution with redshift. Studying stacked mid-infrared (Herschel) data for ultraviolet-selected galaxies in photometric redshift bins at $z \sim 1.5, 3$ and 4, Heinis et al. (2014) identified a strong evolution in their dust extinction with stellar mass, but negligible evolution with redshift. If UV spectral slope is interpreted as varying due purely to dust (as opposed to stellar population age, or metallicity, then this might suggest that somewhere around $z \sim 4-5$ (i.e. when the first galaxies are about 1 Gyr old), the colour evolution stabilises as older stellar populations (and the dust they generate) begin to contribute significantly to the observed colours.

Given that studies such as Heinis et al. (2014) and Burgarella et al. (2011, who studied individually Herschel-detected $z < 2$ examples) suggest a strong luminosity dependence on inferred dust extinction at moderate redshift, while at the highest redshifts Bouwens et al. (2013, 2012) and others have suggested a similar luminosity dependence, it is informative to examine our sample for any similar trend. In figure 5 we plot the rest-frame ultraviolet spectral slope for our sample, as a function of absolute magnitude. As can be seen, the sample probes slopes in the range $-2.5 < \beta < -1.0$, comparable to the typical slopes seen at $z \sim 5 - 7$ (Wilkins et al. 2011, 2013; Douglas et al. 2010; Stanway, McMahon, & Bunker 2005), and shows a similar trend towards bluer slopes at lower luminosities to that suggested in the distant universe. This trend is, admittedly, rather weak in our small pilot sample. Nonetheless, we note that six of our sources (29%) have spectral slopes

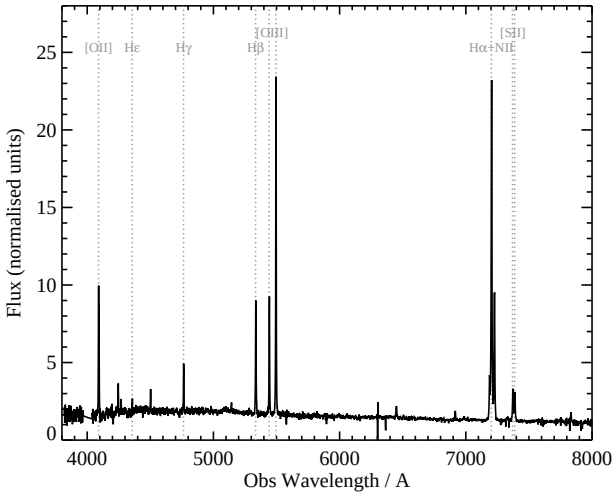

Figure 6. An example of the emission line spectrum typical of these galaxies. Several prominent emission lines related to star formation and metallicity fall into the observed frame optical spectrum. This example lies at $z = 0.097$.

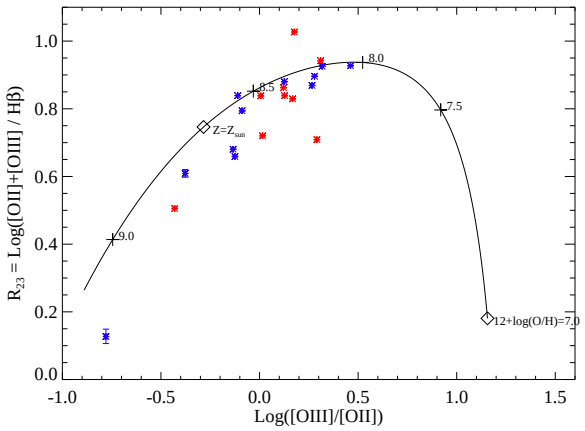

Figure 7. The variation in optical emission line ratios, established as metallicity indicators, in our sample. The solid line shows the mean metallicity as a function of emission line ratio strength in the SDSS galaxy population, calibrated by Maiolino et al 2008 - note that the SDSS galaxy population shows considerable scatter around this mean relation. We adopt a Solar metallicity of 12+log(O/H)=8.69. Galaxies with radio data (see section 4) are shown in red, the remainder of the sample in blue. Formal errors on the measured equivalent widths (propagated to the line ratios) are too small to plot (with a few exceptions), however we note that uncertainty in the continuum for these relatively faint sources may introduce errors at the < 10% (0.05 dex) level. The sources in this sample probe moderate metallicities, with a few outliers.

with $\beta < -1.5$, substantially steeper than that seen in the $z = 3$ population and its analogues ($\beta \sim -0.9$, Shapley et al. 2003).

3.2 Emission Line indices

All the targets in this sample were identified as star-forming galaxies on the basis of their SDSS spectra, and show the typical strong and narrow optical emission lines (see figure 6). In order to evaluate the effectiveness of this sample as LBAs, an important property that must be considered is the metallicity of the dominant stellar population. This is still somewhat poorly constrained at higher redshifts where optical spectroscopy is beyond the grasp of current instruments. As mentioned in the previous section, extremely low metallicities ($< 0.001\,Z_\odot$) have been proposed for the most distant sources, although it is not clear these are strictly necessary.

At $z \sim 5-6$ the metallicity of typical Lyman break galaxies is slightly better known. Fitting of the full spectral energy distribution of photometrically selected galaxies suggest that reasonable fits can be obtained using synthetic stellar populations with metallicities of a few tenths solar (e.g. Verma et al. 2007), while solar metallicity models tend to suggest implausibly old stellar populations at these early times. Similarly, the blue spectral slopes at high redshift, if interpreted as a metallicity indicator yield approximate values of $\sim 0.25\,Z_\odot$ (Douglas et al. 2010). This is consistent with the observed metallicity of absorption line systems in the interstellar medium which is seen to decrease by ~ 1 dex between $z = 0$ and $z = 5$ (and perhaps more rapidly at still higher redshifts, e.g. Rafelski et al. 2012). Similarly, Gamma Ray Burst host galaxies at $z > 4$ (which are believed to be very low mass, Tanvir et al. 2012, , but must be star-forming in order to generate the short-lived GRB progenitors), have been found to have typical metallicities $< 0.15\,Z_\odot$ (see compilation in Thöne et al. 2013).

Thus we would expect good analogues for the distant galaxy population to have metallicities of a few tenths of solar, perhaps decreasing as we search for analogues of galaxies at either higher redshifts or lower luminosities. This is, of course, a crude estimate, and will depend somewhat on the method and species used to make the measurement. We might expect good analogues (which should be young starbursts) to show an enhancement in α-process elements, for example (e.g. Kewley & Ellison 2008).

In figure 7, we plot the classic metallicity indicators R_{23}=([OII]+[OIII])/H_β and log([OIII]/[OII]) for our sample. Line fluxes were extracted from the SDSS spectroscopic catalog for our candidate sources, and tested for consistency against the OSSY determinations by Oh et al. (2011)[3]. Overplotted on figure 7, we show the calibrated empirical relation between these quantities and metallicity from Maiolino et al. (2008). As can be seen, the use of the oxygen ratio can break the well-known metallicity degeneracy in the R_{23} index, placing all of our candidate sample on the upper arm of the metallicity relation. The bulk of our sample (17/21 objects) shows metallicities in the range 8.00 <12+log(O/H)< 8.69 (i.e. $0.2 < Z_\odot < 1.0$, a few tenths Solar). A few outliers in the sample either have higher metallicities or poorly constrained metallicity indices (due to redshifting of one or more emission lines into regions of low signal to noise in the spectroscopy). We note that the blue colours targeted in our sample are clearly possible even at super-Solar metallicities, and will consider the effects of this higher metallicity in individual objects during later analysis.

[3] http://gem.yonsei.ac.kr/∼ksoh/wordpress/?page_id=18

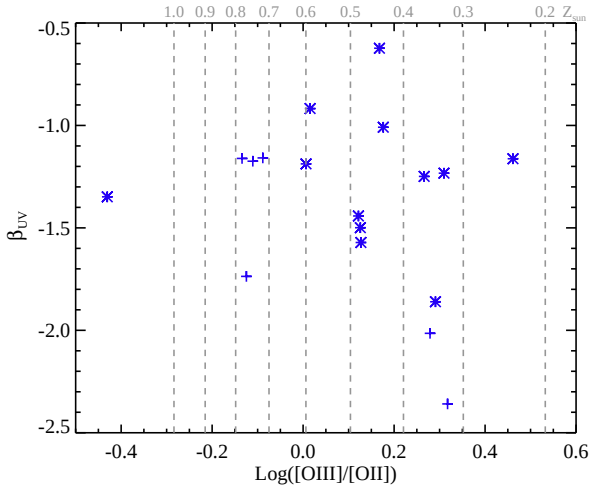

Figure 8. The variation in rest-UV spectral slope β with metallicity (indicated here by the ratio of oxygen emission line strengths) based on the calibration of Maiolino et al 2008 in figure 7. The bulk of this sample probes $0.2 < Z_{\odot} < 0.6$, exploring the same metallicity range inferred for the $z \sim 5$ population. There is tentative evidence for bluer spectral slopes (or at least more dispersion in the spectral slope) with decreasing metallicity.

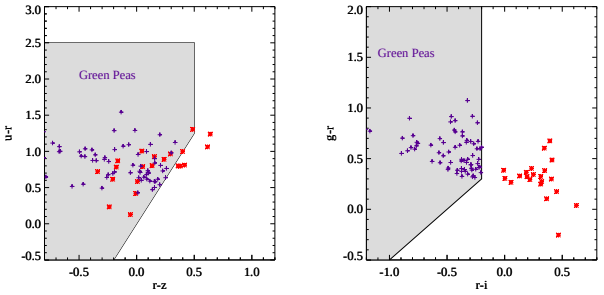

Figure 9. The optical colours of our candidate sample (asterisks), compared to those of the optically-selected 'Green Pea' population identified by Cardamone et al (2009, crosses). Photometric errors are typically smaller than the data points. Our candidates do not satisfy the green pea criteria. Although their spectra are generally blue (as required in the $u-r-z$ colour plane), they do not have the extreme excesses in the r-band identified by the $g-r-i$ colour selection.

However, as figure 8 demonstrates, at least half (11/21 objects) of our sample have measured optical spectral indices consistent with the metallicity range $0.2 < Z_{\odot} < 0.5$ that may be appropriate for high redshift analogues.

Evolution in the rest-frame ultraviolet spectra of distant sources is expected to be driven, at least in part, by evolution in the cosmic mean metallicity at early times. This has been observed between $z = 5$ and $z = 3$ (e.g. Douglas et al 2010), and inferred photometrically at higher redshifts (although with some uncertainty, see Wilkins et al 2013). Figure 8 suggests an intriguing trend is present in our sample. While the number statistics are small, there appears to be a trend towards bluer rest-frame ultraviolet spectral slopes with decreasing metallicity within our sample. Certainly there is a larger dispersion in the spectral slopes for sources at $Z < 0.5 Z_{\odot}$ than for sources around Solar metallicity. However we caution that this sample is too small to disentangle the effects of trends of luminosity (see figure 5) and stellar population age from a pure metallicity evolution. Thus we do not quantify the trend here, due to the small sample statistics, but will investigate this further in future work.

3.3 Optical Colour

In addition to the UV-selected LBA samples discussed above, a second category of local object has been suggested as Lyman break analogues: the optically-selected Green Pea population (Cardamone et al. 2009). These sources are identified from their broad-band photometry as having an excess of flux in the r-band, interpreted as indicative of strong [OIII] emission at $0.112 < z < 0.360$. Hence this selection is designed to identify strongly star-forming galaxies in the local universe.

In figure 9, we compare the optical colours of our candidate sample with Green Peas presented by Cardamone et al. (2009). Our sources do not satisfy the two-fold colour criteria required for identification as Green Peas. Although their spectra are generally blue (as required in the $u-r-z$ colour plane), they do not have the extreme excesses in the r-band identified by the $g-r-i$ colour selection. This is not entirely surprising. The requirement for a very high equivalent width from emission lines in the r-band, but not in the g-band skews the distribution of emission line ratios in the Green Pea sample, and yields galaxies with a mean metallicity of 12-log(O/H)$\sim$ 8.7, rather higher than is typical for our sample, and comparable to Solar metallicity[4]. It also biases the sample to very high star formation rates - with the required line widths giving a typical star formation rate of $\sim 30\,M_{\odot}\,yr^{-1}$. Thus these sources are typically more metal rich and also forming stars at $\sim 3-10$ times the rate of our targets. Given that star formation rate directly influences rest-UV flux, we would also expect the majority of Green Peas to fall outside our ultraviolet luminosity selection, were GALEX data for the whole sample to be available.

Green Peas are selected to be compact in SDSS data (g-band petrosian radius $< 2.0''$, c.f. $< 1.2''$ for our sample), although this requirement translates to a less strict constraint at the high redshift end of their sample. Nonetheless, there would likely be overlap between our sample and the Green Pea selection criteria were we to admit more UV-luminous sources. Those Green Peas which lie towards the low metallicity and lower redshift end of the Cardamone et al and similar selections may well be good analogues for luminous ($L_{UV} > L*_{z=6}$) Lyman break galaxies at high redshift in terms of star formation density. However, the $z \sim 5$ LBA sample presented here remains distinct from the established Green Pea population and is more closely tuned to the properties of relatively faint galaxies currently being identified in deep surveys (see figure 1).

[4] 12-log$(O/H)_{\odot}$ = 8.69 (Allende Prieto, Lambert, & Asplund 2001)

4 RADIO CONTINUUM FOLLOW-UP

Observations at radio wavelengths have the potential to further elucidate the properties of galaxies such as these in two important ways. They can reveal the presence of dust-extincted emission, i.e. a more extended or intense emission source than that seen in the ultraviolet bands where this sample was selected. Detection of a significant excess of emission in radio wavelengths over that predicted from the ultraviolet star formation rate could indicate that the ultraviolet sources are small regions of intense star formation and low extinction embedded in a much larger and more evolved galaxy (Overzier et al. 2010, see also Stanway et al 2010, Davies et al 2012, 2013) and so suggest that these sources would be more analoguous to ULIRG-like super-starbursts than Lyman break galaxies. Alternately, they may indicate the presence of an obscured active galactic nucleus which could substantially effect the evolution and broadband photometry of the system. These two effects are potentially distinguishable based on the radio-frequency spectral slope of any detected emission.

4.1 Observations

We have undertaken an examination of the radio continuum flux at 3 and 6cm wavelengths in a subset of thirteen galaxies, randomly selected from our larger sample of twenty-one targets.

We obtained continuum measurements of the selected galaxies over the period 2012 Aug 27-29, using the Australia Telescope Compact Array (ATCA) in its 6A configuration. The six antennae at the ATCA were aligned along an East-West axis and the longest baselines were 6 km in length. We tuned the Compact Array Broadband Backend (CABB) correlator such that one 2 GHz IF was centered at 5500 MHz (6 cm) and the second at 9000 MHz (3 cm), with full polarization information collected simultaneously at both frequencies. Measurements of PKS 1934-638, the standard calibrator at the ATCA, were used for absolute flux calibration. A bright, compact point source close to each science target was used for atmospheric phase calibration. Our observations were associated with observing programme C2695 (PI: Stanway).

Data were reduced using the dedicated software package MIRIAD (Sault et al. 1995) and radio frequency interference carefully flagged as a function of time on a channel-by-channel basis. Each frequency band had 2048 one MHz-wide spectral channels allowing interference to be restricted to a few distinct channels. This is particularly important at 9000 MHz where powerful interference spikes occurred frequently in certain narrow frequency ranges. Multifrequency synthesis images were constructed from the 2 GHz bandwidth at each frequency. In each image a number of additional sources (often NVSS and occasionally 2MASS objects) were detected. The images were cleaned using a Clark algorithm, constrained to cut off at a level twice the noise standard deviation in the uncleaned images. Uniform weighting was used to optimize suppression of side-lobes in the imaging. All targets were expected to be point sources at the angular resolution of the ATCA.

Short tracks were taken across the full range of possible hour angles, in order to optimize coverage of the *uv*-plane, with a total on-source integration time of 2 hours on each target. These sources are relatively northern for the ATCA. As a result, sources are below the horizon for part of each potential twelve hour earth rotation synthesis track, and the resulting synthesised beam is heavily asymmetric. Typical beam sizes were $\sim 2''$ in right ascension and $\sim 15 - 20''$ in declination at 5500 MHz, with a beam position angle close to zero. Flux uncertainty naturally scales with beam-size for a point source and the noise is heavily correlated between adjacent pixels due to uncertainties in the reconstruction of an incompletely-sampled *uv*-plane.

The MIRIAD task 'imfit' was used to measure the flux and noise levels at the location of the galaxy, which was placed close to the centre of the primary beam ($8.5'$ FWHM at 5500 MHz). Measured fluxes, beam sizes and uncertainties for each target are given in table 1.

4.2 Results

Eight sources are detected at better than 3σ significance in our 5500 MHz data. Of these, the brightest three sources were independently detected in two or more observing sessions, each separated by at least one day. Visual inspection suggests that the weakest detection (in object 05083) is marginal and may or may not be reliable, while a second (object 71294) is similarly faint and has a flux measurement that may be affected by a brighter neighbour. All others appear to be robust detections. None of the eight detected sources are measurably resolved in the radio imaging.

The 9000 MHz band is more heavily affected by noise than that at 5500 MHz. Observations were taken simultaneously in the two bands, and those at 9000 MHz are naturally slightly shallower, although the synthesised beam is smaller by a factor of two. The four brightest sources at 5500 MHz were also detected in the higher frequency data. No other target was significantly detected at 9000 MHz. The results of our radio observations for all targets are given in table 1.

4.3 Radio spectral slope

Table 1 also presents the radio spectral index for those sources with robust detections in one or more wavebands. Where a source is not detected at 9000 MHz, we estimate a limit on the slope based on a limit of 2.5 times the noise level for a point source (at which point detection begins to be plausible in the images).

Radio continuum emission arises as a result either of AGN emission or star formation. While synchrotron emission, arising from electrons accelerated in a strong magnetic field, is ubiquitous in radio sources of all types, the presence of other thermal or non-thermal processes can contribute different emission components, modifying the continuum spectral slope. For example, in ionised hydrogen clouds there is a substantial contribution from free-free or bremstrahlung radiation which arises when unbound electrons are scattered by the magnetic field of nearby ions (see Burke & Graham-Smith 2002, for a full explanation). Hence, where AGN emission dominates, a relatively steep spectral slope is expected, theoretically becoming as steep as $\alpha \sim -2$ for bright quasars with no star formation contribution (Burke & Graham-Smith 2002), and observed values steeper than $\alpha \sim -1$ (e.g. Georgakakis et al. 2012;

Object ID	z	5500 MHz Flux	S/N	Beam size	9000 MHz	S/N	SFR	α
23734	0.108	220 ± 34	6.4	$16 \times 2.0''$	164 ± 31	5.2	5.5 ± 0.9	-0.60 ± 0.15
10880	0.169	86 ± 24	3.6	$18 \times 2.0''$	43 ± 34	1.2	5.5 ± 1.5	<-0.04
19220	0.188	60 ± 82	0.7	$17 \times 2.0''$	44 ± 32	1.4	<13.3	
54061	0.074	215 ± 38	5.6	$19 \times 2.0''$	136 ± 34	4.0	2.5 ± 0.4	-0.93 ± 0.29
60392	0.120	54 ± 26	2.1	$19 \times 1.9''$	73 ± 41	1.8	<1.6	
27473	0.083	57 ± 23	2.5	$16 \times 2.0''$	47 ± 31	1.5	<0.7	
71294	0.146	72 ± 21	3.4	$15 \times 2.0''$	79 ± 53	1.5	3.4 ± 1.0	<1.25
16911	0.097	91 ± 20	4.6	$18 \times 2.0''$	109 ± 27	4.1	1.8 ± 0.4	-0.61 ± 0.12
10045	0.137	69 ± 26	2.6	$15 \times 2.0''$	112 ± 46	2.4	<2.2	
24784	0.113	151 ± 27	5.6	$21 \times 1.9''$	93 ± 43	2.2	4.2 ± 0.7	<-0.70
62100	0.136	61 ± 25	2.4	$20 \times 1.9''$	67 ± 40	1.7	<2.0	
05083	0.146	76 ± 22	3.4	$20 \times 1.9''$	80 ± 32	2.5	3.6 ± 1.0	<0.13
08755	0.164	159 ± 22	7.1	$20 \times 1.9''$	163 ± 33	5.0	9.6 ± 1.3	0.05 ± 0.01

Table 1. Results from the radio observations at 5500 and 9000 MHz, taken at the ATCA. Fluxes and $1\,\sigma$ errors (measured for a point source at the location of the galaxy) are given in μJy/beam. The beam size is given at 5500 MHz and is half this size at 9000 MHz. Measurements with an associated S/N below 3.0 are deemed non-detections. The penultimate column gives the inferred star formation rate in solar masses per year, as described in section 4, with $2\,\sigma$ limits where appropriate. For detected sources, the final column gives the observed-frame 5500MHz/9000MHz spectral index, α, or limit thereupon (based on $2.5\,\sigma$ non-detections at 9000 MHz).

Condon et al. 2013, and references therein). By contrast thermal free-free absorption and emission in star formation regions are expected to flatten the spectrum (particularly at low and high frequencies respectively) by contributing flux with $\alpha \sim -0.1$ and the majority of star forming systems have a fairly shallow slope ($\alpha \sim -0.5 - 0.6$) (see Condon 1992; Berger et al. 2003). Therefore we expect galaxies with ongoing star formation to have moderately negative spectral slopes, and AGN or old stellar populations to be steeper.

Measurements of the spectral index are possible for the four sources detected in both bands of our observations (albeit with substantial uncertainty). Of these, three galaxies have spectral slopes consistent with $-\alpha \sim 0.6 - 0.8$, as expected for faint star-forming sources (see Berger et al. 2003).

The above assumes that we are observing in a frequency regime described by a single, unbroken power law - usually a safe assumption. However aging of the synchrotron-emitting (i.e. relativistic electron) population tends to steepen the radio spectrum above a time-dependent critical value, since high energy electrons decay more quickly than those at lower energies (Condon 1992). This leads to a break in the spectrum which increases in observed frequency with age. In all but the youngest star forming galaxies this break will lie above the frequencies considered here. One source in our sample (object 08755) has a substantially flatter spectral slope than the others, with $\alpha = 0.05$. Spectral slopes this flat are relatively unusual, and may indicate the presence of a spectral break at around ∼6-8 GHz, which would in turn suggest that the source of non-thermal synchrotron emission in this source is very young (Georgakakis et al. 2012).

None of the galaxies in this sample have spectral slopes steep enough to preclude star formation dominated emission, but deeper observations, and observations at more frequencies (both long-wards and short-wards of 5500 MHz) will be necessary to study the radio spectral energy distribution of these sources in more detail.

4.4 Star formation rates

Where robustly detected, and with the possible exception of one object, the radio spectral indices in this sample are consistent with the flux arising from electrons accelerated by supernovae and their remnants. Hence they should track the supernova (and so also star formation) rate.

As a result, radio continuum flux can be straightforwardly converted to an inferred star formation rate given an empirically determined conversion factor. This factor is almost constant for stellar populations forming stars at a constant rate and aged more than about 10^8 years, but can vary for younger stellar populations (Bressan, Silva, & Granato 2002). We calculate the star formation rates inferred from our continuum measurements at 5500 MHz using the same prescription as Berger et al. (2003) and Yun & Carilli (2002). Following Berger et al., we set $\alpha = -0.6$, appropriate for faint radio sources and consistent with those measured in our sample. We use $T_d = 58$ K and $\beta_{\rm FIR} = 1.35$, respectively the dust temperature and emissivity index (again fixed to the values of Yun & Carilli 2002, for comparison with previous studies). At these wavelengths, the thermal dust emission makes a negligible contribution, and setting $T_d = 35$ K and $\beta_{\rm FIR} = 2$ (as found at $z \sim 3$, Davies et al. 2013) has no measurable effect.

Figure 10 illustrates the resultant radio-inferred star formation rates (or limits thereupon) for our sample, in comparison to the star formation rates inferred from their ultraviolet flux[5]. Of the sources with radio detections, the inferred star formation rates derived using the two methods are consistent within a factor of a few, with one source, object 08755, showing a $4.3\,\sigma$ excess in radio continuum, suggesting moderate dust extinction may be reducing the observed ultraviolet flux. We note that this source is an outlier in the sample in several ways: not only does it show a radio excess, it also has a significantly flatter radio spectral slope than those measured in other sources, and is also amongst the reddest sources in the ultraviolet (with $\beta \sim -1$). The sources without radio detections (5/13 targets) are also

[5] Using the same conversion factor applied in figure 1

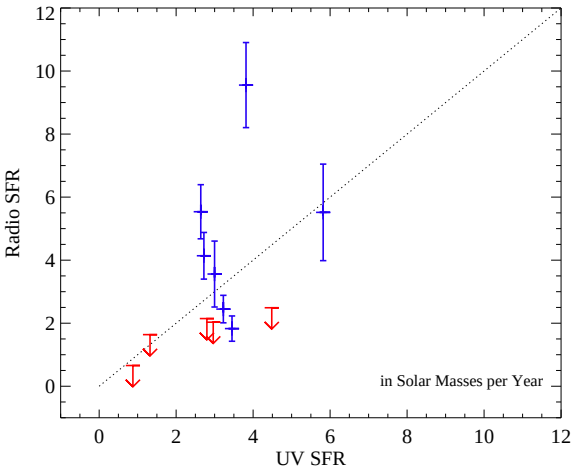

Figure 10. Star formation rates inferred from the GALEX UV (as in figure 1) and ATCA 5500 MHz continuum flux (described in section 4) for the subsample of our targets with ATCA imaging. $2\,\sigma$ limits are shown where a source is undetected. Error bars show uncertainties due to photometric errors, but not systematic uncertainties in the star formation rate conversion factors. The rates are consistent to within a factor of a few both for detected sources and limits. Object 19220, for which relatively weak radio limits were obtained, is omitted from this figure. The star formation rates in these sources are similar to those typical in star forming galaxies at $z > 5$ observed in deep fields. The non-detections at 5500 MHz may indicate young stellar populations, yet to establish a SNe-driven radio continuum in some cases, or that these sources have an unexpectedly steep radio spectral slope.

.

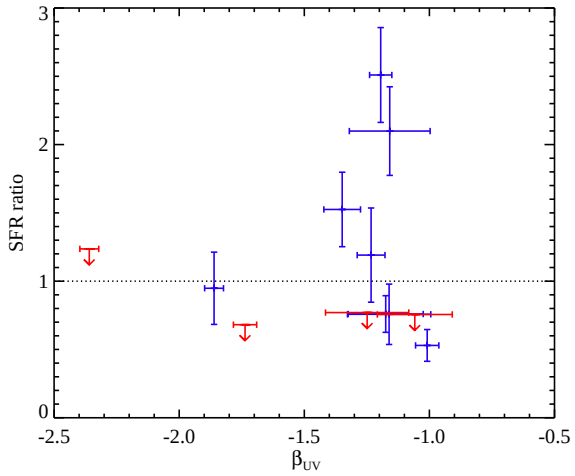

Figure 11. The ratio of star formation rates derived from 5.5 GHz flux to those derived from the ultraviolet (i.e. a source with dusty star formation, or other sources of excess radio emission, would have a ratio greater than one). Where a source is undetected in the radio, $2\,\sigma$ limits are shown. Object 19220, for which relatively weak radio limits were obtained, is omitted from this figure. Four out of eight detections, and three radio limits, are consistent with a deficit in radio flux relative to the ultraviolet.

broadly consistent with their ultraviolet-inferred star formation rates at the $3\,\sigma$ level, although in one case (object 19220), the constraint is relatively weak and this source not considered further here.

However, both the detected fluxes and the limits on undetected objects hint that the radio flux in the typical member of this population may actually be somewhat deficient with respect to their ultraviolet flux. A point source with a flux at least $2.5\,\sigma$ times the background level should have been detected in three of the four cases, and would also likely be accessible to visual inspection, even if formally undetected. Similarly, of the sources that were detected, half (4 out of 8) have measured radio fluxes below those predicted from their UV luminosity (see figure 11). This is a tentative, but potentially interesting result if supported by future observations.

Given the uncertainties in the calibrations applied to derive star formation rates here, it is useful to consider whether alternative indicators might be useful. There is currently no deep near-infrared data available for these sources (which will be surveyed by VISTA over the next few years). As a result, SED fitting becomes ill-constrained and will be explored in a later paper. Data from the WISE survey in the mid-infrared does exist and, particularly in the 22μm W4 band, can also used as a measure of star formation rate over a wide range in luminosity. However, without a deep K-band image to constrain the location of red sources, deconvolution of blended sources in the relatively shallow and low resolution mid-infrared images becomes a substantial problem. As a result, non-detections and extended sources in the WISE catalogues are unlikely to provide useful limits on our targets. Nonetheless, we identify four of our radio-observed sample as relatively isolated and cleanly detected point sources in the "ALLWISE" data release of the W4-band all-sky catalog[6].

Perhaps unsurprisingly, all four detected sources are also well detected in the radio data. We provide a comparison between ultraviolet-, 22μm- and radio-derived star formation rates for these four sources in figure 12, using the star formation rate conversion for the W4 band derived by Shi et al. (2012). As the figure shows, the infrared-derived star formation rates suggest that these sources contain relatively little warm dust, exceeding the ultraviolet-derived values by only $\sim$25%. Interestingly, object 08755 (which has the highest star formation rate in the sample and a flatter than expected radio spectral slope, as discussed in the previous section), does not present as an outlier in this respect, but is consistent with the sample as a whole.

Given that the sources with strong radio detections might usually be expected to be the most massive, and often the dustiest, of our sample, the bulk of the non-detections and blended sources are likely to prove similarly spare of warm dust and until data is available to form a full SED fitting analysis, the ultraviolet-derived star formation rates do not require a substantial dust correction.

As mentioned above, we convert radio flux to star formation using an assumed radio continuum spectral slope $\alpha = -0.6$, consistent with those we measure. Using a steeper spectral slope, $\alpha = -0.75$, results in star formation rate estimates 25% higher. However, even given an adjustment of

[6] http://wise2.ipac.caltech.edu/docs/release/allwise/

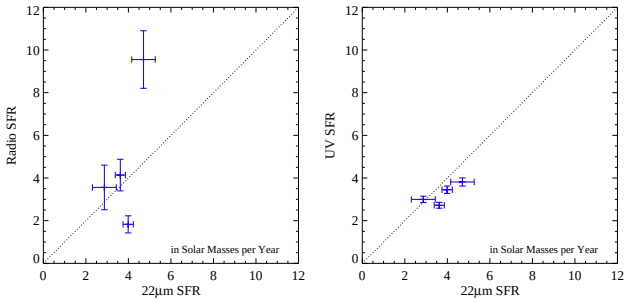

Figure 12. Star formation rates inferred from the WISE 22μm band compared to their ultraviolet and 5500 MHz continuum derived values for the four sources with good WISE detections. Error bars show uncertainties due to photometric errors, but not systematic uncertainties in the star formation rate conversion factors.

this magnitude, six of the sample still show inferred star formation rates lower in the radio than the ultraviolet. Since the few sources bright and isolated enough for WISE detections suggest that the ultraviolet star formation rates might also increase by 25%, the relative deficiency in radio flux remains.

A radio flux in excess of that predicted from the ultraviolet photometry can be straightforwardly interpreted as indicating the presence of dust-obscured star formation. A deficit in the radio emission is more challenging to explain. Any star forming region from which ultraviolet light can escape should present no impediment to the escape of radio photons. Similarly, if the emission was influenced by the presence of an AGN, the radio flux would be expected to exceed that escaping in the ultraviolet. An intriguing possibility is that a deficit in the radio may indicate a very young stellar population. The ultraviolet flux in star forming systems arises from the photospheres of the hottest, most massive stars, with a main sequence lifetime of a few tens of Myr. By contrast, the radio flux is established by supernovae and their remnants at the end of stellar lifetimes, and thus takes longer to stabilize to the standard conversion factors applied.

A young stellar population (<100 Myr, approximately) would be deficient in radio flux (see Bressan, Silva, & Granato 2002). While this could conceivably arise at the onset of continuous star formation, it could also indicate a recent burst, or an exponentially rising star formation rate with cosmic time in these sources (as has been suggested at high redshift by recent modeling and simulation, e.g. Maraston et al. 2010). Any scenario featuring a young, hot stellar population is likely to lead to a bluer intrinsic ultraviolet spectral slope, and thus runs counter to the tentative trend observed in figure 11, which is intriguing. The sources with the bluest spectral slopes in fact show least evidence, one way or the other, for a deficit in radio flux. Since emission from any regions of moderately-dust extincted radio emission should, redden the observed spectral slope, the relatively red ultraviolet colours of the sources with the highest radio excesses are unsurprising. The red colours of the sources with the largest radio *deficits* are rather more so and warrants more investigation. Disentangling the effect of stellar population age and reddening on the spectral slopes in these galaxies will require a full analysis of the ultraviolet through infrared spectral energy distribution of these sources and their spectra and will be investigated in future work.

It is, of course, possible that the radio-deficient galaxies lie just marginally below the detection level in our ATCA observations. Further observations will be required to determine whether these sources are indeed substantially lower in radio flux than expected. If they are indeed young systems, this will strengthen their interpretation as analogues for the generally young systems observed at the highest redshift, and make them potentially useful models for predicting the properties of distant galaxies at submillimetre/radio wavelengths.

5 DISCUSSION AND CONCLUSIONS

In this paper we have presented a new pilot sample of 21 local star forming galaxies that present potential analogues for star forming galaxies in the distant universe - that is, are potential Lyman break analogues for the $z > 5$ galaxy population.

We have demonstrated that these sources provide a good match to the established or expected properties of the distant galaxy population, in terms of star formation density, physical size, ultraviolet luminosity and metallicity, and that they populate a region of these parameter spaces either sparsely populated or unpopulated by existing LBA samples. They show a weak trend towards blue ultraviolet colours at low luminosities and low metallicities that mirrors those seen in the high redshift galaxy population.

Radio continuum investigations preclude the presence of a strong obscured AGN in any of a subsample of 13 sources. Eight sources are detected at a flux level consistent with that expected from their ultraviolet luminosity, assuming that both radio and ultraviolet flux arises from the same star forming population. The remaining sources are undetected in the radio. The relatively low fraction of sources with robust radio detections is intriguing, and, if supported by future observations and forthcoming analysis of their spectral energy distributions, may indicate that these sources are entirely dominated by a very young stellar population.

LBAs such as this may prove extremely useful in interpreting the limited data accessible through observations of faint and heavily redshifted galaxies in the distant Universe. Deep surveys such as CANDELS, and still more so the Hubble Ultra Deep Field campaign and Frontier Fields, are probing a luminosity range, colour selection and star formation density regime that isn't well explored by existing LBA samples. While the number density of these very distant sources, and their photometric colours in the rest-frame ultraviolet, are straightforward to determine, very little detailed information can be extracted from their photometry, and spectroscopy in most cases is limited to Lyman-alpha line emission and weak detections of a low resolution spectral continuum. By contrast, LBAs can be investigated at a full range of wavelengths, from the ultraviolet through to centimetre wavelengths, and detailed abundances and dust properties extracted from optical through near-infrared photometry.

A logical next step in our investigations is to explore the integrated stellar populations in these galaxies - both

through their optical spectroscopy (which is inaccessible in high redshift galaxies) and through analysis of their photometric spectral energy distribution (which is directly comparable to the most commonly-applied technique for analysis of high redshift samples). Forthcoming data from approved LABOCA observations and the VISTA public surveys in the near-infrared, forming a powerful combination with SDSS optical, GALEX ultraviolet photometry and WISE (3-22 μm) imaging should allow tight constraints on dust content, stellar populations and mass to be obtained through fitting of the spectral energy distributions. We also plan to explore their radio, millimetre and far-infrared properties in more detail, now that radio detections have been secured on an initial subsample, and are pursuing an approved programme of integral field spectroscopy in the infrared using SINFONI on the ESO VLT on a subset of objects. This information, will allow us to determine the gas content, dust properties and physical conditions within these young, compact systems, putting them in the wider context of star forming galaxies at low redshifts, and comparing them to the models commonly applied for high redshift star formation.

ACKNOWLEDGMENTS

LJMD acknowledges post-doctoral funding from the UK Science and Technology Facilities Council.

This paper is based in part on data obtained at the Australia Telescope Compact Array associated with programme C2695. The Australia Telescope Compact Array is part of the Australia Telescope National Facility which is funded by the Commonwealth of Australia for operation as a National Facility managed by CSIRO.

It is also based in part on public data from the Sloan Digital Sky Survey DR7. Funding for the SDSS and SDSS-II has been provided by the Alfred P. Sloan Foundation, the Participating Institutions, the National Science Foundation, the U.S. Department of Energy, the National Aeronautics and Space Administration, the Japanese Monbukagakusho, the Max Planck Society, and the Higher Education Funding Council for England. The SDSS Web Site is http://www.sdss.org/. The SDSS is managed by the Astrophysical Research Consortium for the Participating Institutions.

Also based in part on public data from GALEX GR6. The Galaxy Evolution Explorer (GALEX) satellite is a NASA mission led by the California Institute of Technology.

REFERENCES

Abazajian, K. N., Adelman-McCarthy, J. K., Agüeros, M. A., et al. 2009, ApJS, 182, 543
Allende Prieto C., Lambert D. L., Asplund M., 2001, ApJ, 556, L63
Baird S.R., 1981, ApJ, 245, 208
Berger, E., Cowie, L. L., Kulkarni, S. R., et al. 2003, ApJ, 588, 99
Bremer M. N., Lehnert M. D., Waddington I., Hardcastle M. J., Boyce P. J., Phillipps S., 2004, MNRAS, 347, L7
Bouwens R. J., et al., 2013, arXiv, arXiv:1306.2950
Bouwens R. J., et al., 2012, ApJ, 754, 83
Bouwens R. J., Illingworth G. D., Franx M., Ford H., 2007, ApJ, 670, 928
Bressan A., Silva L., Granato G. L., 2002, A&A, 392, 377
Calzetti D., Armus L., Bohlin R. C., Kinney A. L., Koornneef J., Storchi-Bergmann T., 2000, ApJ, 533, 682
Burgarella D., et al., 2011, ApJ, 734, L12
Burke B. F., Graham-Smith F., 2002, "An Introduction to Radio Astronomy: second edition", Cambridge University Press, Cambridge, UK
Cardamone C., et al., 2009, MNRAS, 399, 1191
Condon J. J., 1992, ARA&A, 30, 575
Condon J. J., Kellermann K. I., Kimball A. E., Ivezić Ž., Perley R. A., 2013, ApJ, 768, 37
Davies L. J. M., Bremer M. N., Stanway E. R., Mannering E., Lehnert M. D., Omont A., 2012, MNRAS, 425, 153
Davies L. J. M., Bremer M. N., Stanway E. R., Lehnert M. D., 2013, MNRAS, 433, 2588
Douglas L. S., Bremer M. N., Lehnert M. D., Stanway E. R., Milvang-Jensen B., 2010, MNRAS, 409, 1155
Douglas L. S., Bremer M. N., Stanway E. R., Lehnert M. D., Clowe D., 2009, MNRAS, 400, 561
Douglas L. S., Bremer M. N., Stanway E. R., Lehnert M. D., 2007, MNRAS, 376, 1393
Dunlop J. S., et al., 2013, MNRAS, 432, 3520
Finkelstein S. L., et al., 2012, ApJ, 756, 164
Georgakakis A., Grossi M., Afonso J., Hopkins A. M., 2012, MNRAS, 421, 2223
Grogin, N. A., Kocevski, D. D., Faber, S. M., et al. 2011, ApJS, 197, 35
Haberzettl L., Williger G., Lehnert M. D., Nesvadba N., Davies L., 2012, ApJ, 745, 96
Heckman T. M., et al., 2005, ApJ, 619, L35
Heckman T. M., et al., 2011, ApJ, 730, 5
Heinis S., et al., 2014, MNRAS, 437, 1268
Hoopes C. G., et al., 2007, ApJS, 173, 441
Ibar E., Ivison R. J., Biggs A. D., Lal D. V., Best P. N., Green D. A., 2009, MNRAS, 397, 281
Izotov Y. I., Guseva N. G., Fricke K. J., Henkel C., 2011, A&A, 536, L7
Jia J., Ptak A., Heckman T. M., Overzier R. A., Hornschemeier A., LaMassa S. M., 2011, ApJ, 731, 55
Kewley L. J., Ellison S. L., 2008, ApJ, 681, 1183
Madau P., Pozzetti L., Dickinson M., 1998, ApJ, 498, 106
Maiolino R., et al., 2008, A&A, 488, 463
Maraston C., Pforr J., Renzini A., Daddi E., Dickinson M., Cimatti A., Tonini C., 2010, MNRAS, 407, 830
Maraston C., 2005, MNRAS, 362, 799
Nandra K., Laird E. S., Steidel C. C., 2005, MNRAS, 360, L39
Oesch P. A., et al., 2013, ApJ, 772, 136
Oesch P. A., et al., 2010, ApJ, 709, L21
Overzier R. A., et al., 2011, ApJ, 726, L7
Oh K., Sarzi M., Schawinski K., Yi S. K., 2011, ApJS, 195, 13
Ono Y., Ouchi M., Shimasaku K., Dunlop J., Farrah D., McLure R., Okamura S., 2010, ApJ, 724, 1524
Overzier R. A., Heckman T. M., Schiminovich D., Basu-Zych A., Gonçalves T., Martin D. C., Rich R. M., 2010, ApJ, 710, 979
Rafelski M., Wolfe A. M., Prochaska J. X., Neeleman M., Mendez A. J., 2012, ApJ, 755, 89

Sault, R. J., Teuben, P. J., & Wright, M. C. H. 1995, Astronomical Data Analysis Software and Systems IV, 77, 433
Shapley A. E., Steidel C. C., Pettini M., Adelberger K. L., 2003, ApJ, 588, 65
Shi F., Kong X., Wicker J., Chen Y., Gong Z.-Q., Fan D.-X., 2012, JApA, 33, 213
Stanway E. R., Bremer M. N., Davies L. J. M., Lehnert M. D., 2010, MNRAS, 407, L94
Stanway E. R., McMahon R. G., Bunker A. J., 2005, MNRAS, 359, 1184
Stanway E. R., Bunker A. J., McMahon R. G., 2003, MNRAS, 342, 439
Steidel C. C., Shapley A. E., Pettini M., Adelberger K. L., Erb D. K., Reddy N. A., Hunt M. P., 2004, ApJ, 604, 534
Tanvir N. R., et al., 2012, ApJ, 754, 46
Thöne C. C., et al., 2013, MNRAS, 428, 3590
Verma A., Lehnert M. D., Förster Schreiber N. M., Bremer M. N., Douglas L., 2007, MNRAS, 377, 1024
Wilkins S. M., Bunker A., Coulton W., Croft R., Matteo T. D., Khandai N., Feng Y., 2013, MNRAS, 430, 2885
Wilkins S. M., Bunker A. J., Stanway E., Lorenzoni S., Caruana J., 2011, MNRAS, 417, 717
Yun M. S., Carilli C. L., 2002, ApJ, 568, 88

This paper has been typeset from a TEX/ LATEX file prepared by the author.